Journal of Materials Chemistry A

COMMUNICATION

View Article Online
View Journal

Cite this: DOI: 10.1039/c4ta06394e

Received 24th November 2014
Accepted 26th February 2015

DOI: 10.1039/c4ta06394e

www.rsc.org/MaterialsA

Improving the TiO_2 electron transport layer in perovskite solar cells using acetylacetonate-based additives†

Hsin-Hua Wang,‡[ab] Qi Chen,‡[ab] Huanping Zhou,*[ab] Luo Song,[ab] Zac St Louis,[ab] Nicholas De Marco,[ab] Yihao Fang,[ab] Pengyu Sun,[a] Tze-Bin Song,[ab] Huajun Chen[a] and Yang Yang*[ab]

We developed a facile and quantitative method to improve the electron transport properties and resulting device performances of perovskite solar cells based on post-incorporation of various acetylacetonate additives. Previous studies rely on synthesis or soaking processes with limited additive control. Here, our acetylacetonated-based additives are used as effective intermediate gels to interact with TiO_2 nanocrystals using a simple approach. The incorporation process can be controlled effectively and quantitatively using a range of additives from divalent (II), trivalent (III), and tetravalent (IV) to hexavalent (VI) acetylacetonate. Electronic parameters of solar cell devices, such as short circuit current (J_{sc}) and fill factor (FF), are enhanced, regardless of the different valencies of the additives. Zirconium(IV) acetylacetonate was found to be the most effective additive, with average PCE improved from 15.0% to 15.8%. Detailed characterization experiments including transient photoluminescence spectra, ultra-violet photoelectron spectroscopy, photovoltage decay, and photocurrent decay indicate an improved interface with improved carrier extraction originating from the TiO_2 modification.

Introduction

Hybrid organic–inorganic lead halide perovskites have recently emerged as one of the most promising absorber materials for solar cell applications. Due to their distinct properties that include a high absorption coefficient, an ideal/tuneable band gap and long carrier diffusion lengths, power conversion efficiencies (PCEs) of perovskite solar cells have rapidly increased to ~20%.[1–9] This impressive efficiency, combined with the extremely low cost of raw materials and solution processing, without doubt shows their superiority in thin film technology.[10,11] There have been substantial studies on perovskite absorbers themselves, and the rapid progress mainly stems from the development of processing methods that include one-step solution processes, vapour-assisted solution processes, sequential deposition, co-evaporation, solvent engineering, moisture controlled growth, *etc.*[10,12–18] Meanwhile, it is widely recognized that the interface between the perovskite absorber layer and the carrier transport layer, as well as the properties of the carrier transport layers themselves are also important. An ideal carrier transport material is expected to possess a suitable work function, high conductivity, and low surface recombination rate at the interface. Various materials have been studied as carrier transport layers: *e.g.* TiO_2, ZnO and PCBM as electron transport layers (ETLs) and spiro-OMeTAD, NiO and PEDOT:PSS as hole transport layers (HTLs).[11,19,20] Despite the progress on alternatives, TiO_2 is still the most commonly used ETL and has achieved the best device performance in perovskite devices thus far.[10,21] Consequently, it is important to further investigate TiO_2 to further develop a pathway to boost the PCE of perovskite solar cells.

The initial development of perovskite solar cells relied on 200–500 nm mesoporous TiO_2 structures as ETLs that are usually comprised of nanoparticles with particle sizes around 20 nm. To increase the conductivity of TiO_2, sintering processes at high temperatures around 500 °C are unavoidable.[11] This dramatically increases the complexity of the device fabrication and also reduces its compatibility with flexible substrates, limiting further applications. Subsequent development of perovskite solar cells was based on planar architectures that utilize a compact TiO_2 layer of approximately 40 nm thickness obtained by annealing the titanium precursors or nanocrystals obtained by sol–gel process. Recent studies have reported that titanium diisopropoxide bis(acetylacetonate) ($TiAc_2$) could be used as a gel material between TiO_2 nano-crystals that helps to increase the cross-linkages and the resulting conductivity. Consequently, it also allows the possibility of low temperature solution processing at less than 150 °C to obtain high performance perovskite

[a]Department of Materials Science and Engineering, University of California, Los Angeles, California 90095, USA. E-mail: happyzhou@ucla.edu; yangy@ucla.edu
[b]California NanoSystems Institute, University of California, Los Angeles, California 90095, USA

† Electronic supplementary information (ESI) available. See DOI: 10.1039/c4ta06394e

‡ H. Wang and Q. Chen contributed equally to this work.

solar cells.[22] However, to further improve the electronic properties of TiO_2 materials that are processed at low temperatures, the introduction of extrinsic elements is crucial.

The modification of TiO_2 has been evident in the application of dye-sensitized solar cells (DSSCs), and improved electron transport properties were observed in ETL with proper substitution of Nb^{5+}, Ga^{3+} and Y^{3+}, where Y^{3+} substitution showed the best performance.[23,24] Adopted from DSSCs, researchers also incorporate Y^{3+} to improve the transport properties of TiO_2 in perovskite solar cells by increasing the perovskite loading or passivation of the perovskite/ETL interface.[25,26] The most commonly used route for the incorporation of extrinsic elements into TiO_2 is based on direct synthesis. However, this approach suffers from the complexity of the procedure and limited control of doping concentration. To address this issue, we developed a facile, versatile and quantitative method to introduce extrinsic elements into TiO_2 materials through a post-incorporation approach. Taking Y^{3+} as an example, yttrium(III) acetylacetonate hydrate (YAc_3) was precisely added into $TiAc_2$, and collectively serves as the intermediate gel for the as-prepared TiO_2 nanocrystal. With YAc_3 as the additive, the modified TiO_2 ETL is found to improve the J_{sc} from 19.5 mA cm^{-2} to 20.3 mA cm^{-2}. Additionally, other acetylacetonate-based additives, including bis(acetylacetonato)-dioxomolybdenum(VI) (MoO_2Ac_2), zinc acetylacetonate hydrate ($ZnAc_2$), and zirconium(IV) acetylacetonate ($ZrAc_4$), can be successfully incorporated into TiO_2 nanocrystals with enhanced device performances in terms of J_{sc} and FF. The morphological, structural, optical and electrical properties of the bare ETL film and the resulting devices have been characterized respectively to unveil the underlying mechanisms of the improvement originated from modified TiO_2. It is found that the modified TiO_2, regardless of the valency for different additives, provides a better interface between TiO_2/perovskite, and consequently improves carrier extraction.

Experimental details

Materials

The commercial materials used are listed as follows: PbI_2 (99.999%, Sigma-Aldrich), $TiAc_2$ (75 wt% in isopropanol, Sigma-Aldrich), YAc_3 (Sigma-Aldrich), $ZnAc_2$ (Sigma-Aldrich), $ZrAc_4$ (Sigma-Aldrich), MoO_2Ac_2 (Sigma-Aldrich), spiro-OMeTAD (Lumtec), and ITO substrates.

Precursor synthesis

CH_3NH_3I (MAI) was synthesized by stirring 24 mL of CH_3NH_2 and 10 mL of HI at 0 °C for 2 hours. Using a rotary evaporator, the precipitate was collected by removing the solvents at 50 °C. The product was dissolved in 80 mL anhydrous ethanol and precipitated with the addition of 300 mL diethyl ether. This procedure was repeated twice. The final product was collected and dried at 60 °C in a vacuum oven for 24 h.

The TiO_2 nanocrystals were synthesized by a non-hydrolytic sol–gel approach,[27] where the entire synthetic procedure was performed in ambient air. In a typical synthesis, 0.5 mL $TiCl_4$ was added into 2 mL ethanol slowly with stirring, followed by adding 10 mL benzyl alcohol, leading to a yellow solution. The solution was heated at 80 °C for a period of 5 hours, forming a slightly milky suspension, which was then mixed with 200 mL diethyl ether and centrifuged to collect the precipitate. The as-obtained product was re-dissolved in 30 mL absolute ethanol and precipitated with the addition of 200 mL diethyl ether, and this step was repeated twice. The final TiO_2 was collected and dispersed in ethanol to make a suspension with a concentration of 3–6 mg mL^{-1}. Afterward, $TiAc_2$ was added to the solution, resulting in a solution of 10% weight ratio of TiO_2 to $TiAc_2$.

The additives, including YAc_3, $ZnAc_2$, $ZrAc_4$ and MoO_2Ac_2, were first dissolved in anhydrous ethanol, and then added to the TiO_2/$TiAc_2$ mixture in a weight ratio of 0.05–0.1%. The solution was stored in the refrigerator after each use.

X-ray diffraction

Samples for X-ray diffraction patterns were prepared by dripping TiO_2 precursor solution onto a glass substrate and a 2θ–θ X-ray diffraction scan was collected using a powder X-ray diffractometer (Panalytical X'Pert Pro) using Cu-K_α radiation ($\lambda = 1.54050$ Å).

Conductivity measurement

Conductivity measurements were conducted by a two-point measurement using two aluminium metal electrodes on a TiO_2 (or additive incorporated TiO_2) layer with thicknesses around 40 nm. The channel length was 200 μm and the width was 1 mm.

Device fabrication

Under ambient environment, the ITO substrates were cleaned with diluted detergent, deionized water, acetone and isopropanol in an ultrasonic bath in sequence. These substrates were then spin-coated with pure TiO_2 precursor solution at 3000 rpm for 30 seconds and baked at 150 °C for 15 minutes on a hot plate. After the first layer of TiO_2, TiO_2 precursor solutions with different additives were spin-coated onto the substrate under the same conditions, followed by baking at 150 °C for 30 minutes. For the perovskite layer, PbI_2 solution of concentration 450 mg mL^{-1} in DMF was coated on the substrate in a dry air glove box while the PbI_2 solution was kept stirring at 70 °C. MAI:MACl was then coated on the PbI_2 layer. MAI:MACl mixed solution was prepared by dissolving 50 mg MAI and 5 mg MACl in 1 mL isopropanol. The samples were then baked in ambient atmosphere at 135 °C for 10 minutes and returned to the dry air glove box. The hole transport layer (HTL) was then coated on the sample. The precursor of the HTL was prepared by using 1 mL spiro-OMeTAD/chlorobenzene (90 mg mL^{-1}) solution with addition of 15 μL Li-TFSI/acetonitrile (210 mg mL^{-1}), and 40 μL tBP. Finally, 110 nm gold was deposited as a bottom electrode using a thermal evaporator under a pressure of 2×10^{-5} Torr.

Photovoltaic characterization

The current density–voltage (J–V) curves were measured using a Keithley 2401 source-measure unit under AM1.5G illumination

at 100 mW cm^{-2} provided by an Oriel Sol3A solar simulator in ambient environment. The light intensity was carefully calibrated using a calibrated KG-5 filter diode. During the measurement, the photovoltaic devices were masked by a metal aperture to confine the active area (0.10 cm^2).

Steady state and transient photoluminescence spectrum

The steady-state photoluminescence (PL) spectrum was recorded using a Horiba Jobin Yvon system with an excitation at 633 nm. The time-resolved photoluminescence spectrum was acquired using the time-correlated single-photon counting technique (Picoharp 300), and the excitation light pulse was provided using a picosecond diode laser at a wavelength of 633 nm with a repetition frequency of 1 MHz (PDL 800B).

Photovoltage and photocurrent decay

A white light bias was generated from an array of diodes (Molex 180081-4320). A nitrogen laser (LSI VSL-337ND-S, 337 nm) was used as the perturbation source, with a pulse width of 4 ns and a repetition frequency of 10 Hz. The intensity of the perturbation laser pulse was controlled to maintain the amplitude of transient V_{oc} below 5 mV so that the perturbation assumption of excitation light holds. The voltages under open circuit and currents under short circuit conditions were measured over a 1 MΩ and a 50 Ω resistor, and were recorded on a digital oscilloscope (Tektronix DPO 4104B).

Results and discussion

Device performance based on Y^{3+} modified TiO_2

We take Y^{3+} as an example to examine the effects originating from extrinsic ion incorporation into the carrier transport materials. Previous work has suggested that Y^{3+} can be incorporated into TiO_2 through direct synthesis of TiO_2 nanocrystals with certain amounts of substituent reactants, *e.g.* $TiCl_4$. However, the formation of nanocrystals is highly dependent on the reaction kinetics, *e.g.* reaction time and temperature, resulting in varied doping levels of extrinsic ions into TiO_2. Thus, it is difficult to accurately control the content of dopants into the TiO_2 layer, which hampers a systematical study on the ETL materials and the corresponding devices. In the current approach, the additives (*e.g.* YAc_3) were directly added into the original intermediate $TiAc_2$, and post incorporated into the TiO_2 nanocrystal solution. To form the ETL, the solution was spin-coated and then annealed at 150 °C for a period of 30 minutes. This approach utilizes the positive effects of the interaction between the intermediate (*e.g.* $TiAc_2$) and TiO_2 nanocrystals for improving the conductivity of the TiO_2 layer, which is confirmed by previous studies.[22] It is expected that the incorporation of additives into the $TiAc_2$ will further improve the electronic properties of the carrier transport materials.

J–V measurements of Y^{3+} modified TiO_2 materials are shown in Fig. 1 and Table 1. A comparison of *J–V* parameters between TiO_2 and (0.05% wt) Y–TiO_2 is shown in Fig. 1a. Both samples exhibit a comparable open-circuit voltage (V_{oc}) of 1.017 V and fill factor (FF) of 74.5%, while the short circuit current (J_{sc}) based on Y–TiO_2 improved from 19.5 mA cm^{-2} to 20.3 mA cm^{-2}, when compared to the reference TiO_2-based device. Consequently, we observed an increased device performance from 14.5% to 15.4% power conversion efficiency (PCE). This is consistent with previous studies showing that Y–TiO_2 benefits the J_{sc} and the resulting PCE. The concentration of incorporated YAc_3 has also been studied to assess its influence on device performance. To achieve a statistic result, we provided 8–12 nominally identical devices for each condition. According to Fig. 1b, the quantity of YAc_3 incorporation is critical to the device performance. The measured PCE is maximized when the weight ratio of YAc_3/TiO_2 is adjusted in the range of 0.05% to 0.1%, and dropped significantly when the weight ratio was further increased to 0.4%. This indicates that too high a concentration of Y^{3+} is detrimental to device performance, possibly due to increased trap

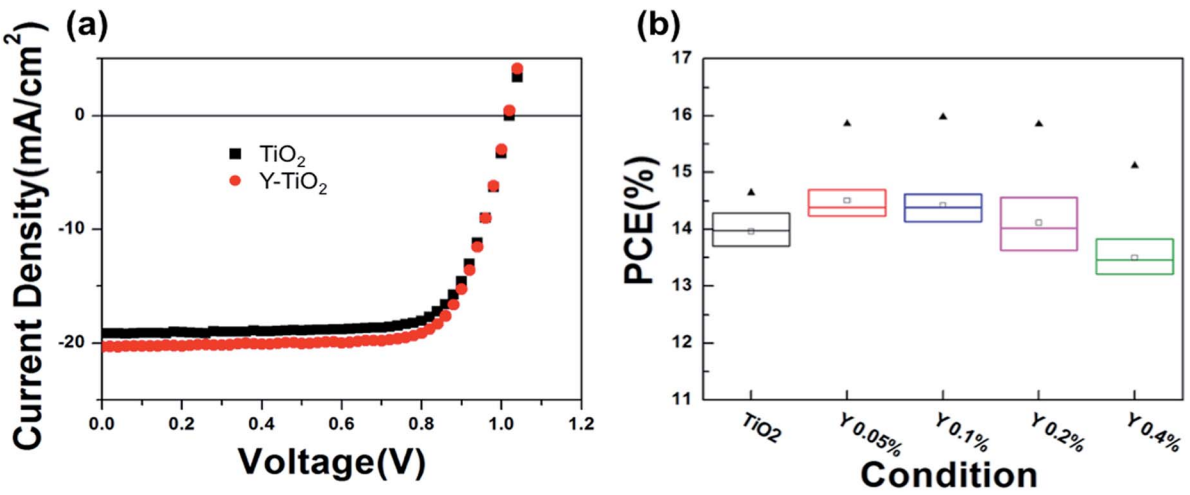

Fig. 1 (a) Typical device *J–V* curve of the TiO_2 ETL incorporated with YAc_3. (b) Devices statistics of the PCE based on different concentrations of YAc_3 incorporated into the TiO_2 ETL. The three horizontal lines in the box indicate the 25th, 50th and 75th percentile of devices. The triangle and the hollow squares represent the highest and the average value, respectively.

Table 1 Device performance of the ETL incorporated with different additives

Additives	V_{oc} (V)	J_{sc} (mA cm^{-2})	PCE (%)	FF (%)
w/o additive	1.025	19.5	15.0	75.0
0.05% YAc_3	1.017	20.2	15.4	74.8
0.1% $ZnAc_2$	1.024	20.1	15.6	76.0
0.1% $ZrAc_4$	1.021	20.3	15.7	76.6
0.1% MoO_2Ac_2	1.009	20.0	15.4	76.0

states in the as-prepared Y–TiO_2 or the Y–TiO_2/perovskite interface. A detailed investigation on the mechanism will be discussed later.

XRD measurement

X-ray diffraction patterns (XRD) were used to investigate the structure of the modified TiO_2 materials. As shown in Fig. 2, the resulting materials exhibit a clear anatase phase, centered at 25.0°, 37.5°, and 47.4°, corresponding to a TiO_2 crystal. No crystal structural transformation was observed even when the additive concentration weight ratio was increased to 0.4%. Incorporation of additives thus does not have an apparent effect on the crystal structure. This suggests that moderate annealing of TiO_2 materials is not sufficient for effective doping of TiO_2 with acetylacetonate-based precursors. It could also be reasonable to infer that the additive has a negligible effect on the structural properties of the nano-crystal, since the incorporation process is conducted after the synthesis of the TiO_2 nano-crystals. Thus, the additives may act as an intermediate material between nano-crystals.

Device statistics for other additives

We further investigated the versatility of this approach by incorporating a series of other additives into the TiO_2 nano-crystals. These additives include MoO_2Ac_2, $ZnAc_2$ and $ZrAc_4$.

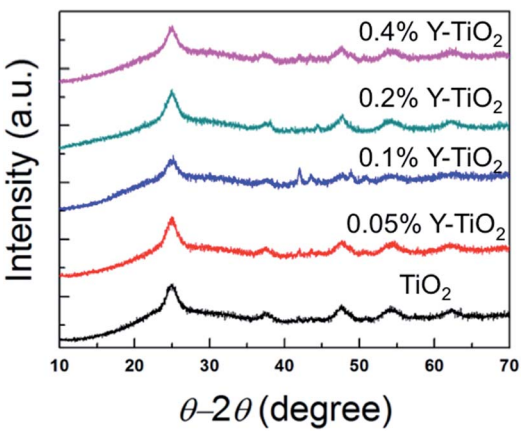

Fig. 2 X-ray θ–2θ scan of the TiO_2 ETL incorporated with different concentrations of YAc_3.

Fig. 3 shows a statistical representation of device performance based on different TiO_2 ETL modifications. Accordingly, we found that all devices based on modified TiO_2 exhibit superior J_{sc} and FF, when compared with the reference. The average J_{sc} was increased from 20 (mA cm^{-2}) to around 20.5 (mA cm^{-2}) for the modified samples, while, the FF increased from 75% to 76.5%. In regard to V_{oc}, all devices show a comparable V_{oc} of around 1.02 V, except for those based on Mo–TiO_2. As a result, the four different additives produced enhanced PCEs from 15.0% to 15.5–15.8%. It is worth mentioning that devices based on Zr–TiO_2 still possess the highest device performance, with an apparent enhancement of both J_{sc} and FF. This result in part agrees with previous findings in thin film solar cells demonstrating that the introduction of extrinsic ions into TiO_2 benefits device performance, particularly the J_{sc}.[25] The suggested reason for the enhanced J_{sc} was associated with an increased loading amount of the absorber or improved carrier transport characteristics of the ETL. Previous studies on perovskite solar cells indicate that yttrium acts as the most effective additive into TiO_2, and that the mechanism lies in the enhanced material loading and passivation of the TiO_2 surface.[25,26] Our present work shows that the best device performances are achieved with Zr^{4+} additives. This further invokes a deeper understanding of the underlying mechanism of the modified ETL materials in perovskite solar cells.

To investigate the origin of enhanced device performance *via* incorporation of additives in TiO_2 ETLs, we characterized the effects of both the absorber layer and across the heterojunction.

Absorption spectrum

Material loading on the ETL layer can affect the current density and device performance. It is reported that in a mesoporous structure, yttrium substituted TiO_2 showed an improvement in J_{sc}, attributed to better material loading.[25] To this end, we measured the absorption spectrum of the perovskite absorber layer grown on different TiO_2 ETLs. According to the results shown in Fig. S1,† there is no detectable difference in absorption spectra for different perovskite materials. This indicates that the modified TiO_2 has a negligible effect on material loading of perovskite. This also suggests a difference between planar and mesoporous structures, where for planar structures the J_{sc} enhancement does not result from the increased material loading arising from modified TiO_2.

Conductivity

The conductivity of pristine TiO_2 and the modified TiO_2 was measured through two-point measurements, and the results are shown in Table 2. Incorporation of MoO_2Ac_2, $ZnAc_2$, YAc_3, $ZrAc_4$ into the TiO_2 film largely increased its conductivity when compared to the pristine TiO_2 film. The measured conductivity of the ETL is in the range of 1×10^{-4} to 4×10^{-4} (S cm^{-1}), which is lower compared to reported values. We attributed this to the contact resistance originating from the two-point measurement setup.[22] Among all the additives, $ZnAc_2$ shows the most striking improvement, where the conductivity increased from 1.42×10^{-4} to 3.72×10^{-4} (S cm^{-1}). The enhanced

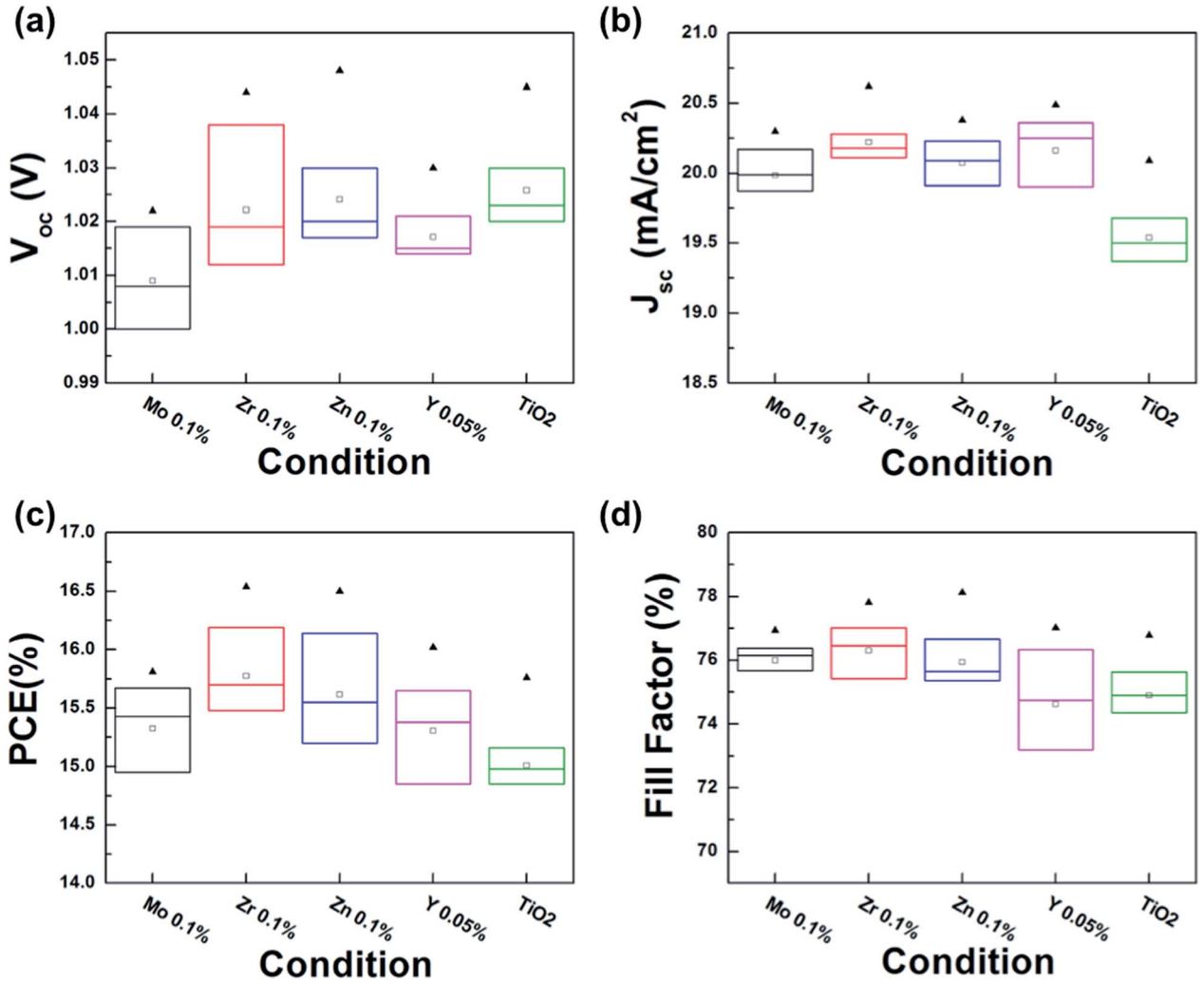

Fig. 3 Device statistics of (a) V_{oc}, (b) J_{sc}, (c) PCE and (d) fill factor of the perovskite solar cell employing the ETL incorporated with different acetylacetonate-based additives. The three horizontal lines in the box indicate the 25th, 50th and 75th percentile of devices. The triangle and the hollow squares represent the highest and the average value, respectively.

conductivity of the ETL layer could possibly help to improve carrier transport and subsequently benefit the J_{sc} and FF, which is in accordance with our device performance.

Fermi energy

Ultraviolet photoelectron spectroscopy (UPS) was used to extract the Fermi energy of the ETL materials. With addition of acetylacetonate-based additives, the Fermi energy levels of TiO_2 were shifted from pure TiO_2 (4.0 eV) to Zn–TiO_2 (3.85 eV), Y–TiO_2 (3.9 eV), Zr–TiO_2 (4.18 eV) and Mo–TiO_2 (4.1 eV), respectively, as shown in Fig. S2.† It was found that the variation of the Fermi energy of electron transport materials covers a wide range of ~0.33 eV from Zn–TiO_2 to Zr–TiO_2. Generally, the Fermi energy shift is associated with the changed carrier concentration, and the doping effect plays a very important role. However, given that the concentration of additives in TiO_2 are at the level of 10^{-5} in the current study, a 0.33 eV Fermi energy change cannot arise simply from the varied carrier concentration. In addition, the Fermi energy shift does not follow the tendency of valency change, which further suggests that bulk doping is not the major factor responsible for the Fermi energy shift. As all device parameters have been improved due to the incorporation of extrinsic elements regardless of the element valency, we

Table 2 Conductivity of additive incorporated TiO_2 ETL

	w/o additives	0.05% YAc_3	0.1% MoO_2Ac_2	0.1% $ZnAc_2$	0.1% $ZrAc_2$
Conductivity (S cm^{-1})	1.42×10^{-4}	2.60×10^{-4}	2.32×10^{-4}	3.72×10^{-4}	1.86×10^{-4}

therefore consider that the improved device performance is closely related to surface properties, *e.g.* surface passivation, rather than the Fermi energy.

Transient photoluminescence spectra

Time-resolved photoluminescence (TRPL) was then used to characterize the perovskite absorber layer grown on various TiO_2 ETLs. TRPL is a common approach used to extract the carrier lifetime (τ), which is a direct indication of the various radiative and nonradiative loss channels responsible for photoexcited carrier recombination. All the samples exhibit τ values in the range of 80 to 102 ns. Considering its exceptional carrier mobility, this allows a carrier diffusion length of over 1 μm, which is sufficient for the carrier to be extracted across the whole film thickness of approximately 350 nm. However, slightly different carrier lifetimes were observed in these samples, decreasing from: $ZrAc_4$, $ZnAc_2$, MoO_2Ac_2, and YAc_3, as shown in Table 3. It is reported that non-radiative recombination mainly arises from two major competing processes regarding charge transport, namely, carrier recombination ($\tau_{perovskite}$) and charge-carrier transfer (τ_{CT}), following the relationship $1/\tau_{heterojunction} = 1/\tau_{perovskite} + 1/\tau_{charge\ transfer}$.[2] In the current study, the lifetime is calculated based on two-exponential decays, and the 2nd component is considered to be indicative of the carrier recombination of perovskite. Thus, it could be deduced that the ETL can affect the quality of perovskite materials, and the corresponding carrier behavior. The relatively high carrier lifetime of $ZrAc_4$ most likely also agrees with the improved performance, as discussed above.

Table 3 TRPL lifetime of the PVSK/ETL structure

	w/o additives	0.05% YAc_3	0.1% $MoAc_2$	0.1% $ZnAc_2$	0.1% $ZrAc_2$
Lifetime (ns)	87	80	81	96	102

Photocurrent and photovoltage decay

To study the origin of the improved device characteristics from the modified TiO_2 materials, we investigate the carrier dynamics along the entire pathway in the completed cells based on transient photovoltage and photocurrent measurements. As shown in Fig. 4a, all devices based on improved TiO_2 showed rapid photocurrent decay when compared to the reference cell, indicating the additives in the ETL largely benefit the photocarrier extraction from the perovskite absorber layer. The transport lifetimes of photocarriers in the complete devices as a function of illumination intensity are shown in Fig. 4b. The lifetimes are well-fitted by a single exponential curve, indicating that charge extraction from the perovskite absorber layer is the dominant recombination pathway. Electron transport lifetimes have accordingly been found to be noticeably different for the devices employing ETL additives. The decay lifetimes are 1.79, 1.62, 1.48 and 1.36 (μs), for the MoO_2Ac_2, $ZnAc_2$, $ZrAc_4$, and YAc_3 modified TiO_2-based samples, respectively, compared with the undoped TiO_2 decay lifetime of 2.20 μs under the same intensity

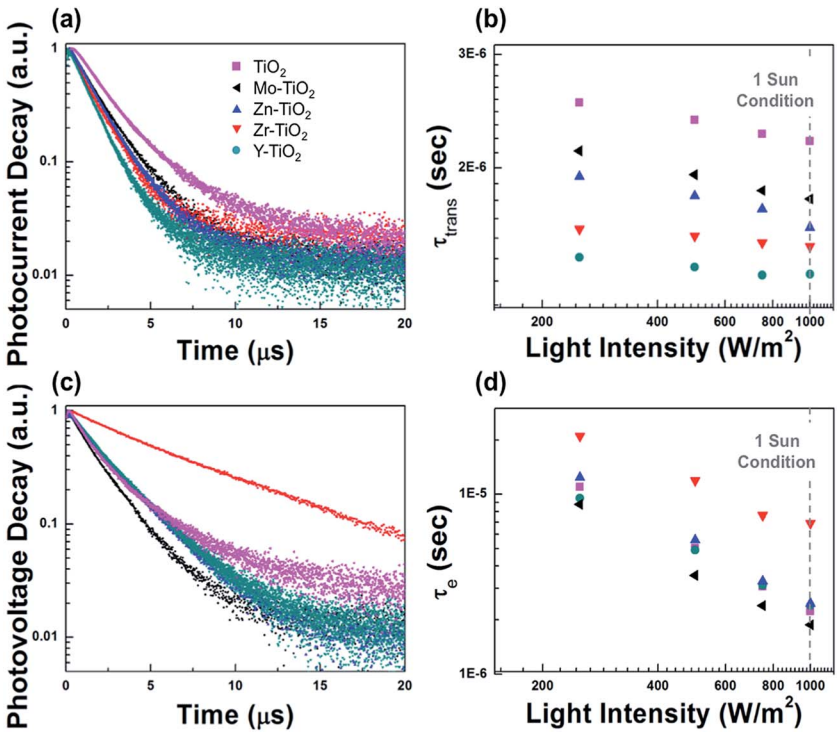

Fig. 4 Photocurrent and photovoltage decay of devices employing the TiO_2 ETL incorporated with different acetylacetonate-based additives and the related carrier transport lifetime and electron lifetime. Intensity is shown in log scale and 1 sun condition is equivalent to 1000 W m^{-2}.

of biased white light. Among the four additives, the YAc_3 modified ETL showed the most rapid photocurrent decay, in accordance with highest J_{sc} observed in Fig. 3b. Transient photovoltage measurements (as shown in Fig. 4c), which correlate with the electron lifetime in the absorber, provide insight into carrier recombination rates within the cell. Contrarily to transient photocurrent decay, not all of the four modified samples show prolonged photovoltage decay. We further extracted the electron lifetimes from light intensity dependent photovoltage decay measurements for complete devices, as shown in Fig. 4d. The decay lifetimes were 7.01, 2.48, 2.40, and 1.88 (μs), for $ZrAc_4$, $ZnAc_2$, YAc_3 and MoO_2Ac_2 modified TiO_2 samples, respectively, compared with pristine TiO_2 decay lifetime of 2.23 μs for the same intensity of biased white light. It is in accordance with the observation of slow microsecond time scale recombination at ambient solar intensities,[28–30] suggesting that carrier recombination is predominately limited by the perovskite layer. This result also reveals that modified TiO_2 ETLs may affect trap densities in the perovskite material or at the interfaces. Interestingly, it is also in excellent agreement with carrier lifetimes, as shown in TRPL measurements, where devices based on Zr–TiO_2 as the ETL had the longest electron lifetimes, while devices based on Mo–TiO_2 had the shortest electron lifetimes. This further influences the electrical characteristics of the device, particularly V_{oc}, as both TRPL and transient photovoltage decay measurements largely correlate with recombination in perovskite materials.

The above investigation suggests that the modified TiO_2 can generally improve the carrier extraction in perovskite devices, which benefits the J_{sc} and FF, and eventually the PCE. It should be noticed that the additives incorporated into the TiO_2 materials can be varied from Zn^{2+}, Y^{3+}, and Zr^{4+} to Mo^{6+}. Additionally, all the additives can help to improve the conductivity of TiO_2. Given that improved properties of TiO_2 can be achieved by incorporating any kind of metals, regardless of the valency, it rules out the doping mechanism as the source of the improvement. This is also in correspondence with the unchanged crystal structure of the modified TiO_2 materials (Fig. 2). Absorption spectra also exclude the possibility of increased loading amounts of perovskite materials (Fig. S1†) and morphological changes (Fig. S4†) of the ETL responsible for improved J_{sc}. Thus, we infer that the positive effect of the additives may be associated with the possible passivation of defect states either within the bulk or at interfaces, consistent with the reported study.[26] This mechanism can further explain the reduced carrier recombination in perovskite materials arising from TiO_2 additives. All devices exhibited slight hysteresis to a similar degree (Table S1†), which indicates that additive incorporation does not significantly affect the physical contact between the ETL materials and perovskite materials. The stability of perovskite solar cells (Fig. S6†) shows a random trend, where the devices based on Mo–TiO_2 exhibit improved stability, while others perform decreased stability when compared to standard TiO_2 devices. Further investigation of the origin of the improved device performances seen in the modified TiO_2 films and underlying degradation mechanisms are underway.

Conclusions

In summary, we successfully demonstrated a general, facile and quantitative approach to improve the TiO_2 ETL in perovskite solar cells, with enhanced device performances, particularly pertaining to short circuit current (J_{sc}) and fill factor (FF). Our method is based on post-synthesis incorporation of acetylacetonated-based additives into TiO_2 nanocrystals, facilitated by the interaction between the intermediate gel and nanocrystals. The acetylacetonate additives consist of elements of varying valencies ranging from Zn(II), Y(III), and Zr(IV) to Mo(VI). The underlying mechanism of the modified TiO_2 and the corresponding improved device performances were investigated carefully and attributed to better carrier extraction. This approach can be extended to other systems, such as ZnO, through systematically engineering nanocrystals with selected additives or dopants. Future progress will be focused on investigating the mechanisms of transient charge transfer within the modified TiO_2 and absorber films. More importantly, the continuous advances on extrinsic element incorporation will enable highly efficient and flexible photovoltaic devices.

Acknowledgements

This work was supported financially by the National Science Foundation (NSF-ECCS 1202231, Program Manager: Dr Paul Werbos), Air Force Office of Scientific Research (grant no. FA9550-12-1-0074, Program Manager: Dr C. Lee), and UCLA internal funds.

Notes and references

1 S. D. Stranks, G. E. Eperon, G. Grancini, C. Menelaou, M. J. P. Alcocer, T. Leijtens, L. M. Herz, A. Petrozza and H. J. Snaith, *Science*, 2013, **342**, 341–344.
2 G. Xing, N. Mathews, S. Sun, S. S. Lim, Y. M. Lam, M. Grätzel, S. Mhaisalkar and T. C. Sum, *Science*, 2013, **342**, 344–347.
3 C. Wehrenfennig, M. Liu, H. J. Snaith, M. B. Johnston and L. M. Herz, *Energy Environ. Sci.*, 2014, **7**, 2269.
4 A. Marchioro, J. Teuscher, D. Friedrich, M. Kunst, R. van de Krol, T. Moehl, M. Grätzel and J.-E. Moser, *Nat. Photonics*, 2014, **8**, 250–255.
5 W.-J. Yin, T. Shi and Y. Yan, *Adv. Mater.*, 2014, **26**, 4653–4658.
6 J. M. Frost, K. T. Butler, F. Brivio, C. H. Hendon, M. van Schilfgaarde and A. Walsh, *Nano Lett.*, 2014, **14**, 2584–2590.
7 H. Snaith, *J. Phys. Chem. Lett.*, 2013, **4**, 2423–2429.
8 N. Park, *J. Phys. Chem. Lett.*, 2013, **4**, 3623–3630.
9 C. Wehrenfennig, G. E. Eperon, M. B. Johnston, H. J. Snaith and L. M. Herz, *Adv. Mater.*, 2014, **26**, 1584–1589.
10 H. Zhou, Q. Chen, G. Li, S. Luo, T.-B. Song, H.-S. Duan, Z. Hong, J. You, Y. Liu and Y. Yang, *Science*, 2014, **345**, 542–546.
11 J. M. Ball, M. M. Lee, A. Hey and H. J. Snaith, *Energy Environ. Sci.*, 2013, **6**, 1739.
12 J. You, Y. Yang, Z. Hong and T. Song, *Appl. Phys. Lett.*, 2014, **105**, 183902.

13 Q. Chen, H. Zhou, Z. Hong, S. Luo, H.-S. Duan, H.-H Wang, Y. Liu, G. Li and Y. Yang, *J. Am. Chem. Soc.*, 2014, **136**, 622–625.
14 J. Burschka, N. Pellet, S.-J. Moon, R. Humphry-Baker, P. Gao, M. K. Nazeeruddin and M. Grätzel, *Nature*, 2013, **499**, 316–319.
15 N. Jeon, J. Noh, Y. Kim, W. Yang, S. Ryu and S. Seok, *Nat. Mater.*, 2014, 1–7.
16 M. Liu, M. B. Johnston and H. J. Snaith, *Nature*, 2013, **501**, 395–398.
17 J. You, Z. Hong, Y. M. Yang, Q. Chen, M. Cai, T. Song and C. Chen, *ACS Nano*, 2014, **8**, 1674–1680.
18 Q. Chen, H. Zhou, T.-B. Song, S. Luo, Z. Hong, H.-S. Duan, L. Dou, Y. Liu and Y. Yang, *Nano Lett.*, 2014, **14**, 4158–4163.
19 P. Docampo, J. M. Ball, M. Darwich, G. E. Eperon and H. J. Snaith, *Nat. Commun.*, 2013, **4**, 2761.
20 J.-Y. Jeng, K.-C. Chen, T.-Y. Chiang, P.-Y. Lin, T.-D. Tsai, Y.-C. Chang, T.-F. Guo, P. Chen, T.-C. Wen and Y.-J. Hsu, *Adv. Mater.*, 2014, **26**, 4107–4113.
21 A. Yella, L.-P. Heiniger, P. Gao, M. K. Nazeeruddin and M. Grätzel, *Nano Lett.*, 2014, **14**, 2591–2596.
22 K. Wojciechowski, M. Saliba, T. Leijtens, A. Abate and H. J. Snaith, *Energy Environ. Sci.*, 2014, **7**, 1142.
23 A. K. Chandiran, L. Etgar and M. Graetzel, *J. Phys. Chem. C*, 2011, 0–8.
24 A. K. Chandiran, F. Sauvage, M. Casas-Cabanas, P. Comte, S. M. Zakeeruddin and M. Graetzel, *J. Phys. Chem. C*, 2010, **114**, 15849–15856.
25 P. Qin, A. L. Domanski, A. K. Chandiran, R. Berger, H.-J. Butt, M. I. Dar, T. Moehl, N. Tetreault, P. Gao, S. Ahmad, M. K. Nazeeruddin and M. Gratzel, *Nanoscale*, 2014, **6**, 1508–1514.
26 Y. Ogomi, K. Kukihara, S. Qing, T. Toyoda, K. Yoshino, S. Pandey, H. Momose and S. Hayase, *ChemPhysChem*, 2014, **15**, 1062–1069.
27 J. Wang, J. Polleux, J. Lim and B. Dunn, *J. Phys. Chem. C*, 2007, **2**, 14925–14931.
28 V. Roiati, S. Colella, G. Lerario, L. De Marco, A. Rizzo, A. Listorti and G. Gigli, *Energy Environ. Sci.*, 2014, **7**, 1889.
29 R. S. Sanchez, V. Gonzalez-Pedro, J.-W. Lee, N.-G. Park, Y. S. Kang, I. Mora-Sero and J. Bisquert, *J. Phys. Chem. Lett.*, 2014, **5**, 2357–2363.
30 A. Baumann, K. Tvingstedt, M. C. Heiber, S. Väth, C. Momblona, H. J. Bolink and V. Dyakonov, *APL Mater.*, 2014, **2**, 081501.

